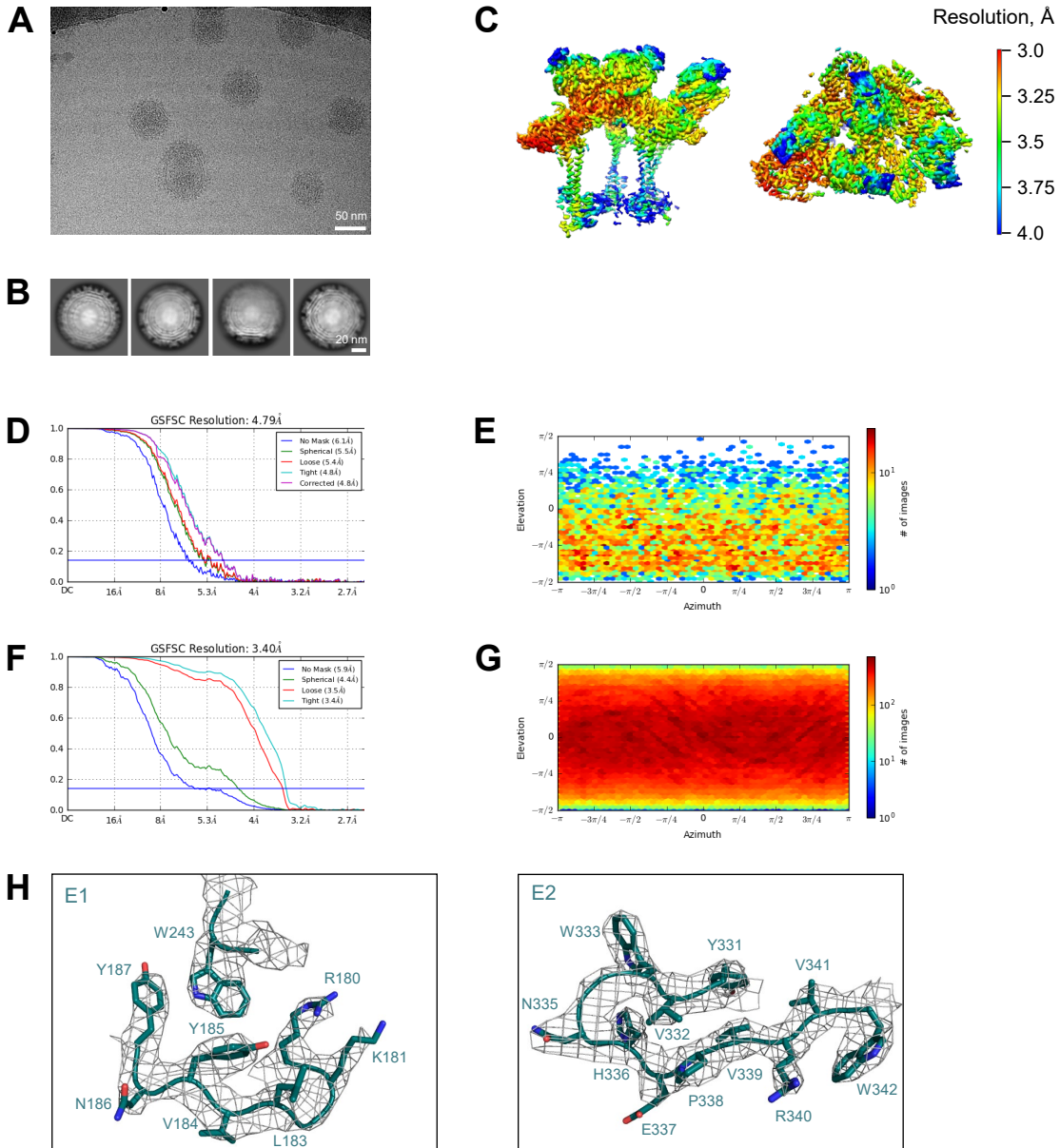# Data S1. Cryo-EM validation for VLPs and VLP-Fab complexes, related to Figures 4-6.
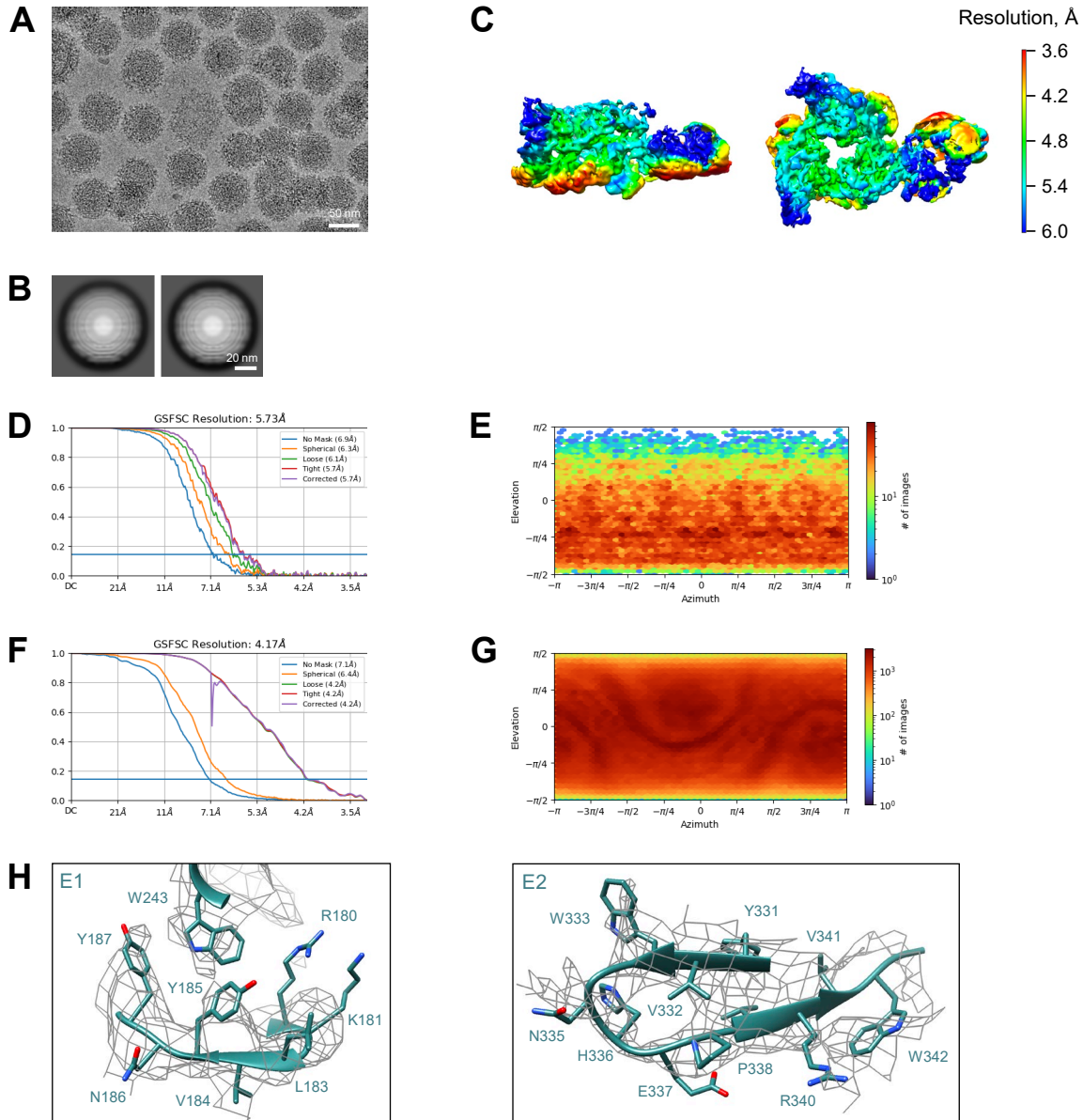
## Table of contents for Data S1

**Data S1. Cryo-EM validation of WEEV VLP, related to Figures 4-6.**

(A) Representative micrograph. (B) Representative 2D class averages. (C) The local resolution map. (D) The gold-standard Fourier shell correlation for the whole WEEV VLP after global refinement. (E) Heatmap showing the orientations of all WEEV VLP particles used in the global refinement. (F) The gold-standard Fourier shell correlation for the asymmetric unit of WEEV VLP after symmetry expansion and focused refinement. (G) Heatmap showing the orientations of all WEEV VLP particles used in the focused refinement. (H) Electron density for selected parts of the E1 and E2 proteins after focused refinement contoured at 3.4 σ.
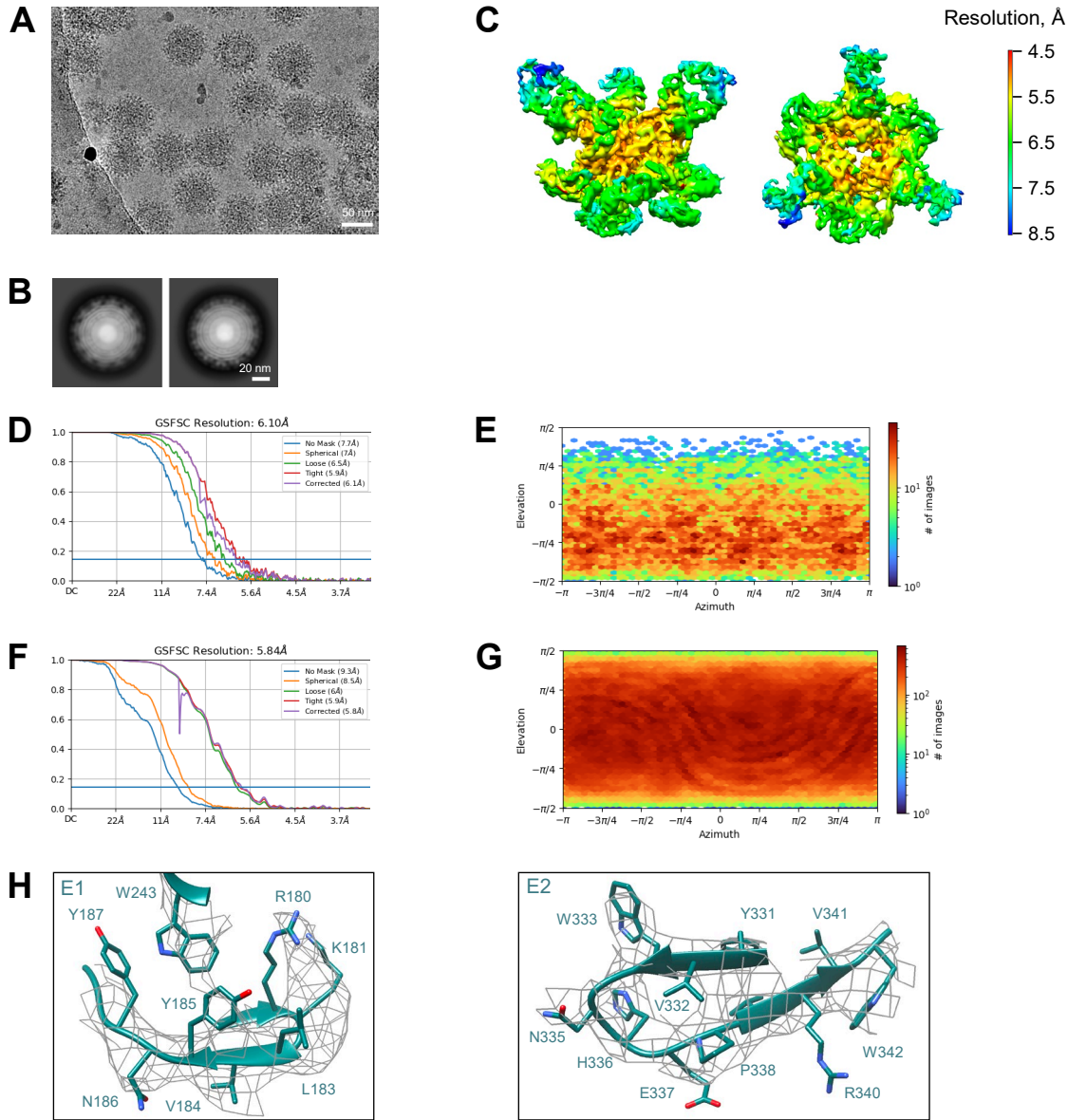
**Data S1. Cryo-EM validation of SKT05-WEEV VLP, related to Figures 4-6.**
(A) Representative micrograph. (B) Representative 2D class averages. (C) The local resolution map. (D) The gold-standard Fourier shell correlation for the entire complex after global refinement. (E) Heatmap showing the orientations of all particles used in the global refinement. (F) The gold-standard Fourier shell correlation for the asymmetric unit of the complex after symmetry expansion and focused refinement. (G) Heatmap showing the orientations of all particles used in the focused refinement. (H) Electron density for selected parts of the E1 and E2 proteins after focused refinement contoured at 1.4 σ.

**Data S1. Cryo-EM validation of SKW11-WEEV VLP, related to Figures 4-6.**
(A) Representative micrograph. (B) Representative 2D class averages. (C) The local resolution map. (D) The gold-standard Fourier shell correlation for the entire complex after global refinement. (E) Heatmap showing the orientations of all particles used in the global refinement. (F) The gold-standard Fourier shell correlation for the asymmetric unit of the complex after symmetry expansion and focused refinement. (G) Heatmap showing the orientations of all particles used in the focused refinement. (H) Electron density for selected parts of the E1 and E2 proteins after focused refinement contoured at 2.1 σ.
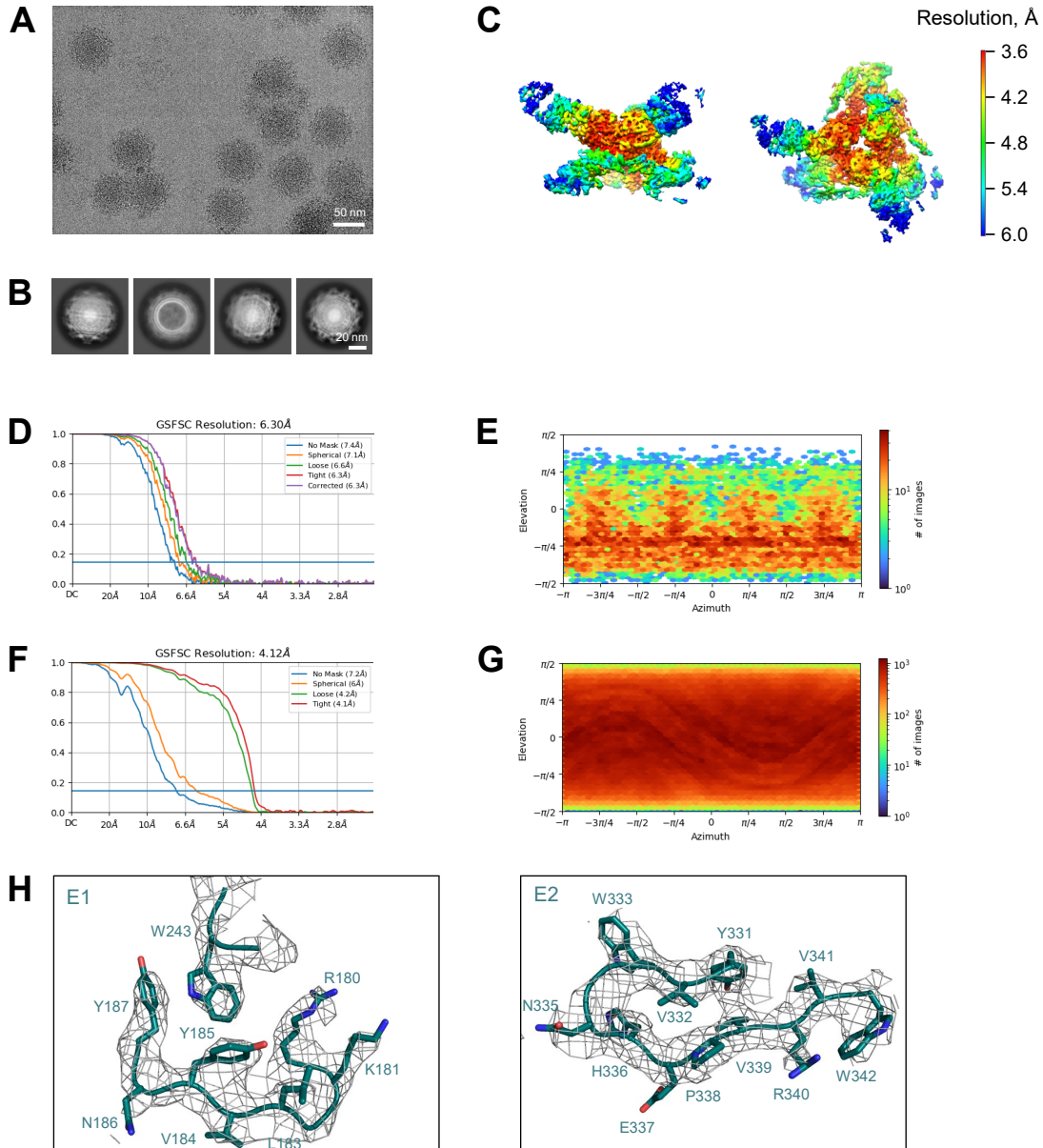
**Data S1. Cryo-EM validation of SKW19-WEEV VLP, related to Figures 4-6.**
(A) Representative micrograph. (B) Representative 2D class averages. (C) The local resolution map. (D) The gold-standard Fourier shell correlation for the entire complex after global refinement. (E) Heatmap showing the orientations of all particles used in the global refinement. (F) The gold-standard Fourier shell correlation for the asymmetric unit of the complex after symmetry expansion and focused refinement. (G) Heatmap showing the orientations of all particles used in the focused refinement. (H) Electron density for selected parts of the E1 and E2 proteins after focused refinement contoured at 3.4 σ.
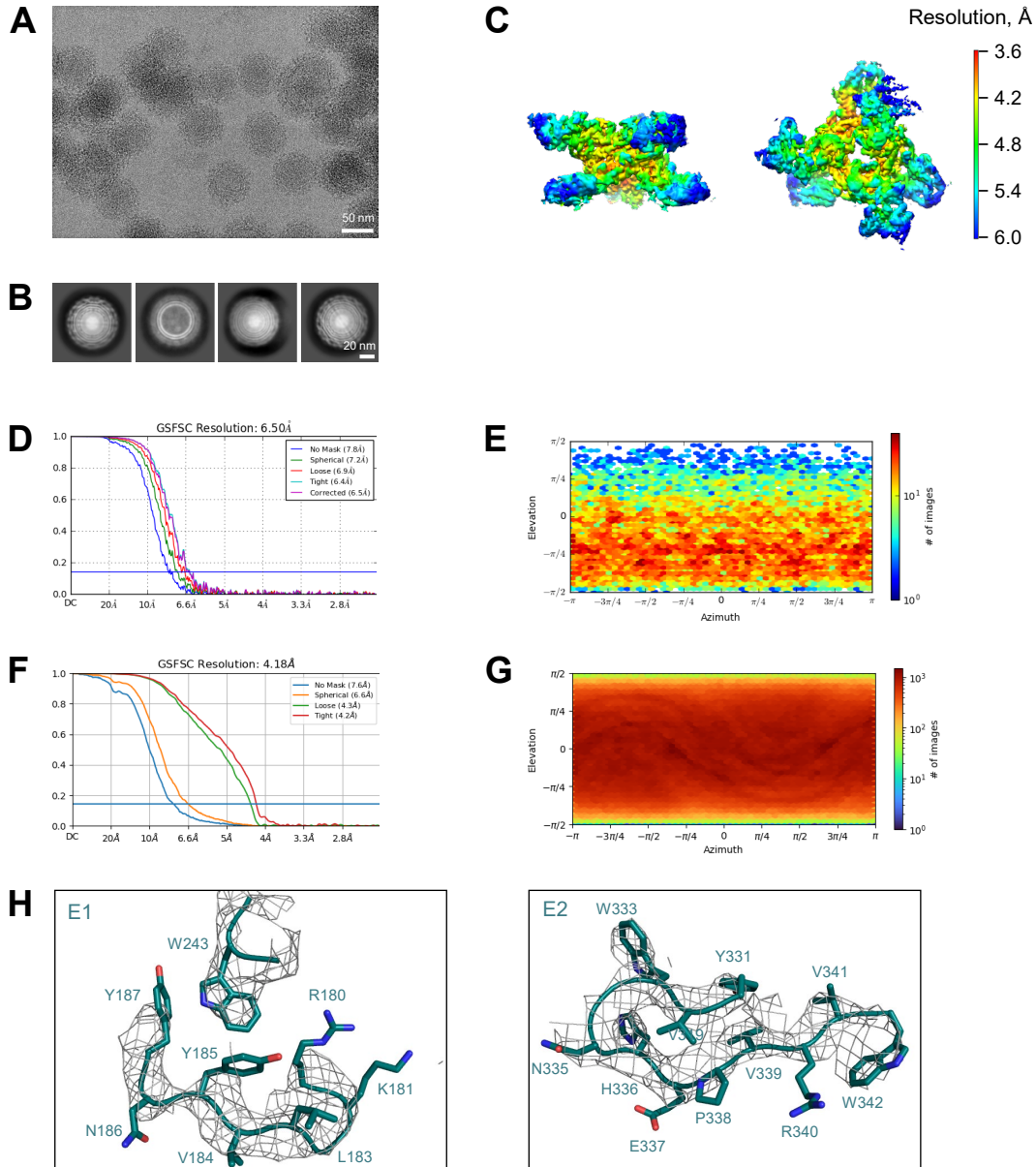
**Data S1. Cryo-EM validation of SKW24-WEEV VLP, related to Figures 4-6.**
(A) Representative micrograph. (B) Representative 2D class averages. (C) The local resolution map. (D) The gold-standard Fourier shell correlation for the entire complex after global refinement. (E) Heatmap showing the orientations of all particles used in the global refinement. (F) The gold-standard Fourier shell correlation for the asymmetric unit of the complex after symmetry expansion and focused refinement. (G) Heatmap showing the orientations of all particles used in the focused refinement. (H) Electron density for selected parts of the E1 and E2 proteins after focused refinement contoured at 3.4 σ.
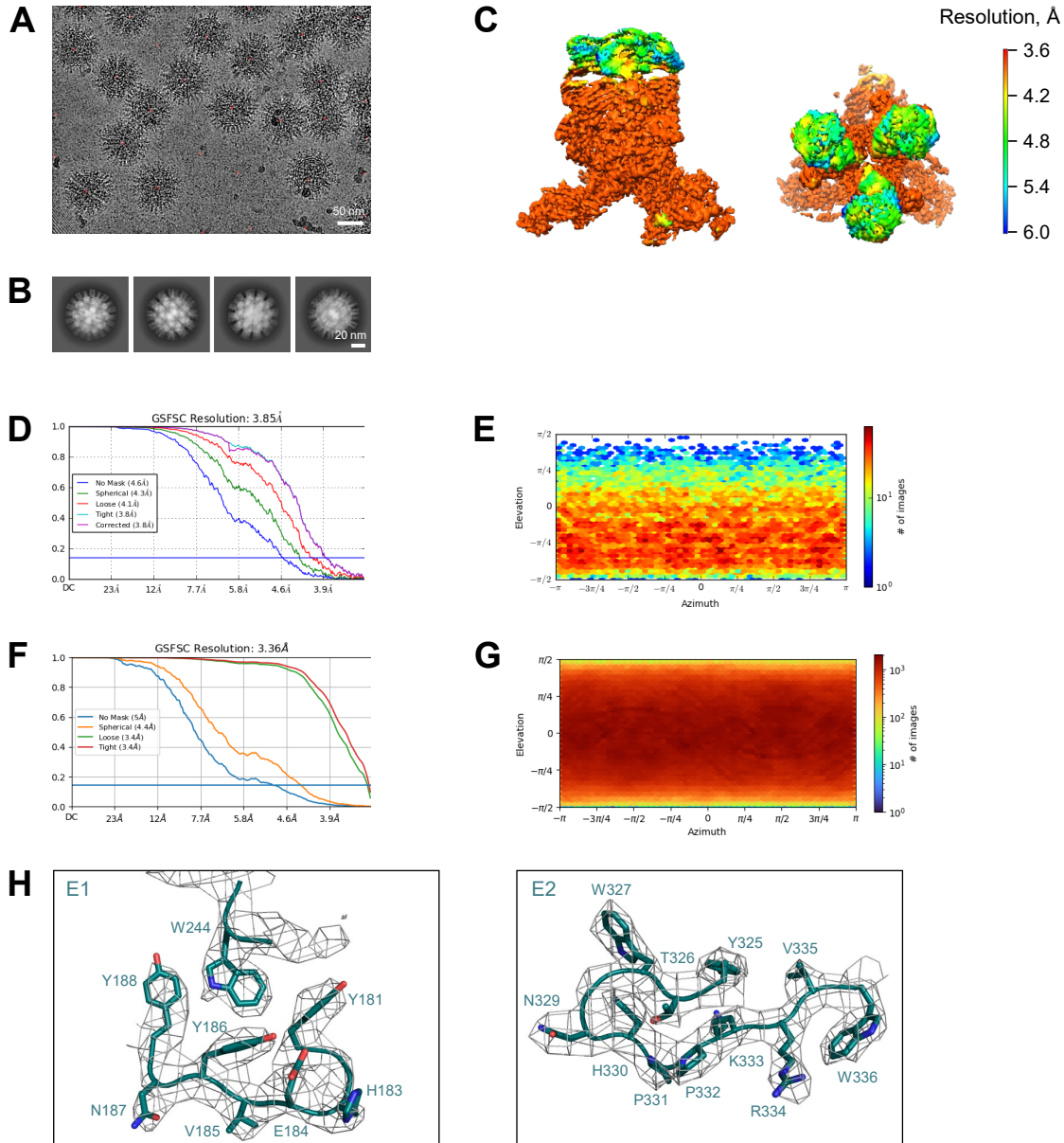
**Data S1. Cryo-EM validation of SKE26-EEEV VLP, related to Figures 4.**

(A) Representative micrograph. (B) Representative 2D class averages. (C) The local resolution map. (D) The gold-standard Fourier shell correlation for the entire complex after global refinement. (E) Heatmap showing the orientations of all particles used in the global refinement. (F) The gold-standard Fourier shell correlation for the asymmetric unit of the complex after symmetry expansion and focused refinement. (G) Heatmap showing the orientations of all particles used in the focused refinement. (H) Electron density for selected parts of the E1 and E2 proteins after focused refinement contoured at 14.0 σ.
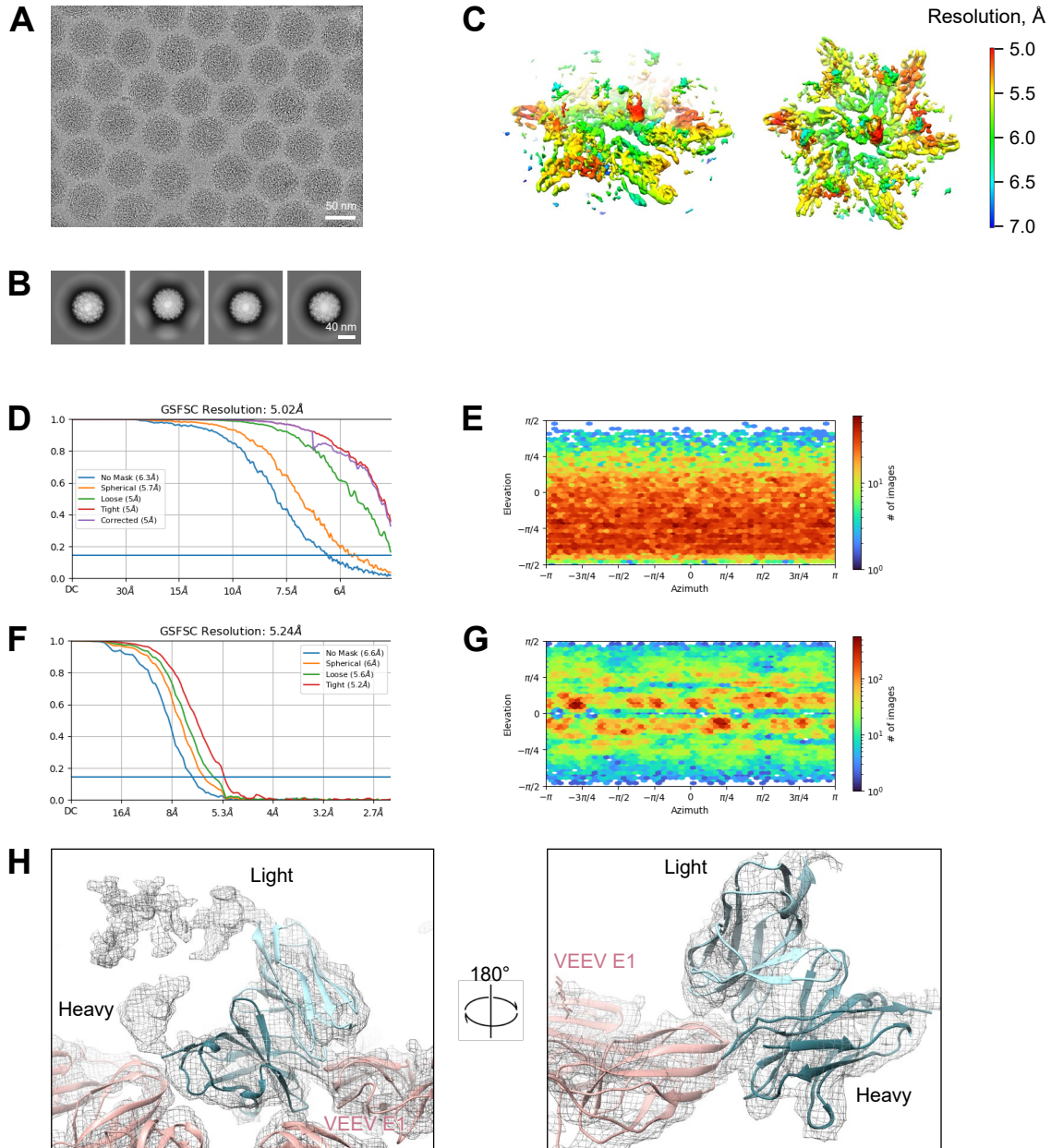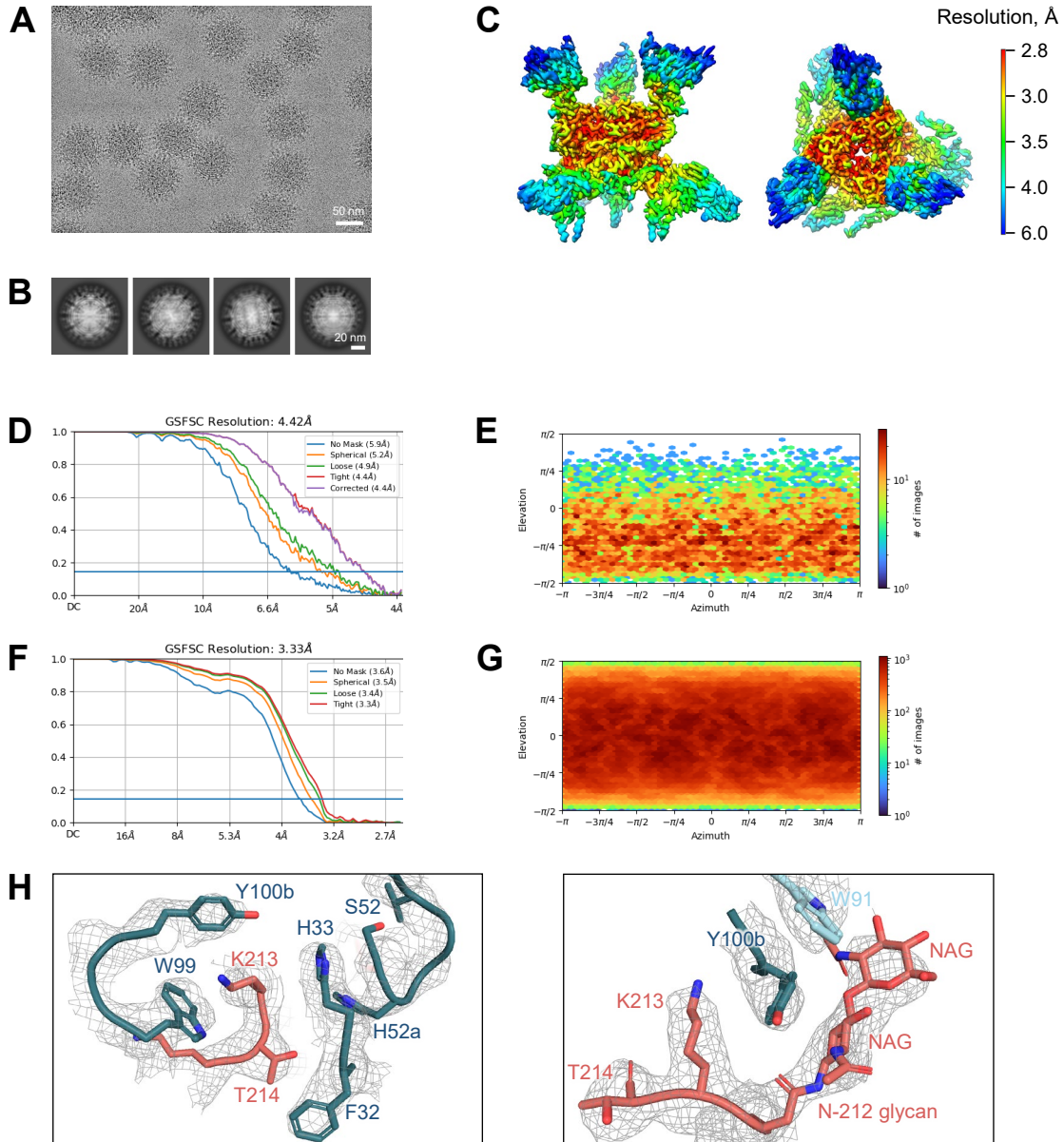
**Data S1. Cryo-EM validation of SKV09-VEEV VLP, related to Figures 4-6.**
(A) Representative micrograph. (B) Representative 2D class averages. (C) The local resolution estimation mapped onto local SKV09-VEEV subparticle reconstruction. (D) The gold-standard Fourier shell correlation for the whole SKV09-VEEV VLP with I1 symmetry applied. (E) Heatmap showing the projection orientations of all SKV09-VEEV VLP icosahedral particles used in the refinement. (F) The gold-standard Fourier shell correlation for VEEV E1 proteins in complex with SKV09 after symmetry expansion, focused classification, and local refinement. (G) Heatmap showing the orientations of all symmetry expanded SKV09-VEEV subparticles used in the local refinement. (H) Electron density for the antibody interface after local refinement.
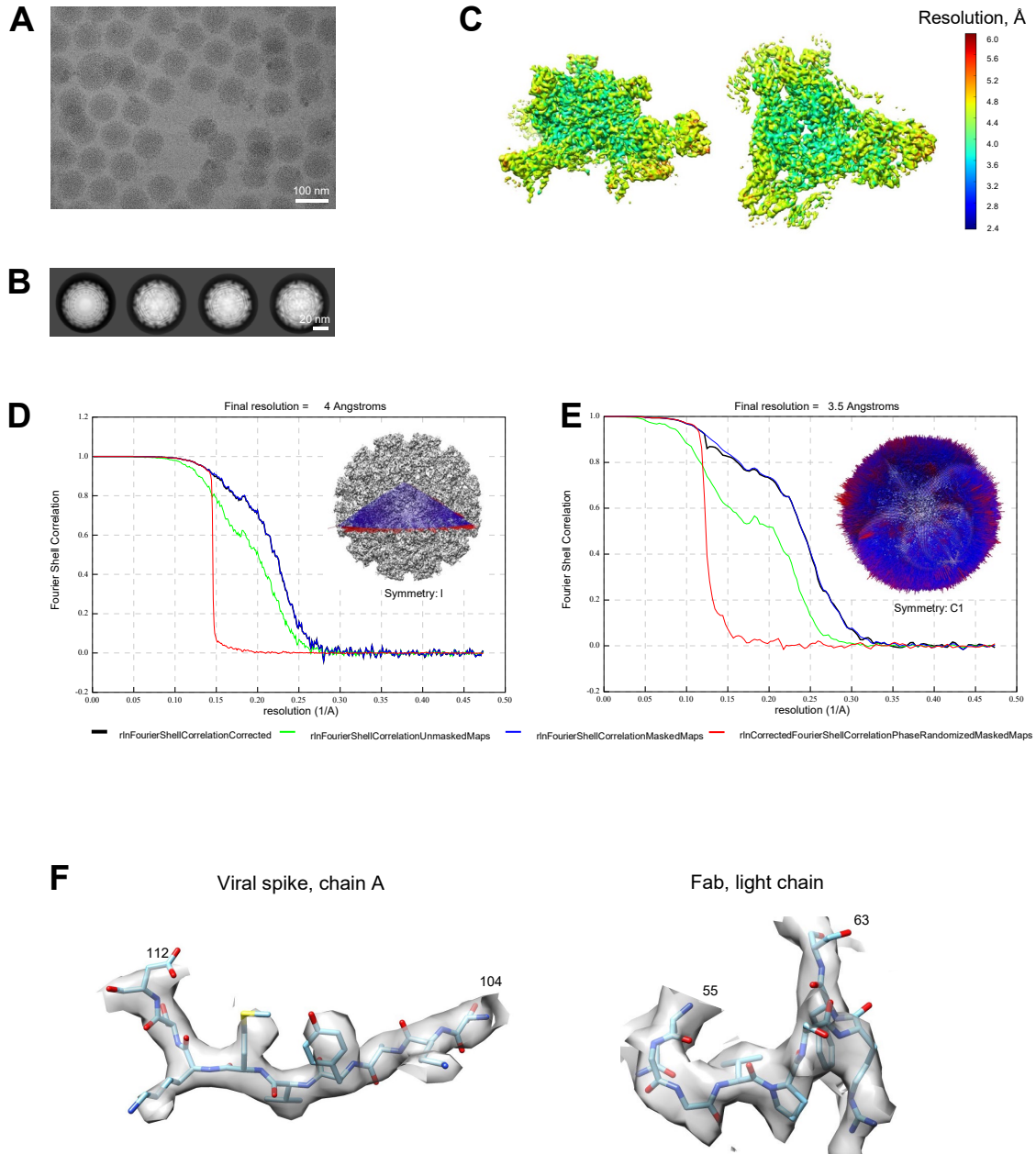
**Data S1. Cryo-EM validation of SKV16-VEEV VLP, related to Figures 4-6.**
(A) Representative micrograph. (B) Representative 2D class averages. (C) The local resolution estimation mapped onto local SKV16-VEEV subparticle reconstruction.
(D) The gold-standard Fourier shell correlation for the whole SKV16-VEEV VLP with I1 symmetry applied. (E) Heatmap showing the projection orientations of all SKV16-VEEV VLP icosahedral particles used in the refinement. (F) The gold-standard Fourier shell correlation for the spike of VEEV in complex with SKV16 after symmetry expansion and local refinement. (G) Heatmap showing the projection orientations of all symmetry expanded SKV16-VEEV subparticles used in the local refinement. (H) Electron density for selected interactions on the antibody interface after local refinement.

**A**

100 nm

**C**

Resolution, Å

6.0
5.6
5.2
4.8
4.4
4.0
3.6
3.2
2.8
2.4

**B**

20 nm

**D**

Final resolution = 4 Angstroms

Fourier Shell Correlation

resolution (1/A)

Symmetry: I

**E**

Final resolution = 3.5 Angstroms

Fourier Shell Correlation

resolution (1/A)

Symmetry: C1

— rlnFourierShellCorrelationCorrected    — rlnFourierShellCorrelationUnmaskedMaps    — rlnFourierShellCorrelationMaskedMaps    — rlnCorrectedFourierShellCorrelationPhaseRandomizedMaskedMaps

**F**
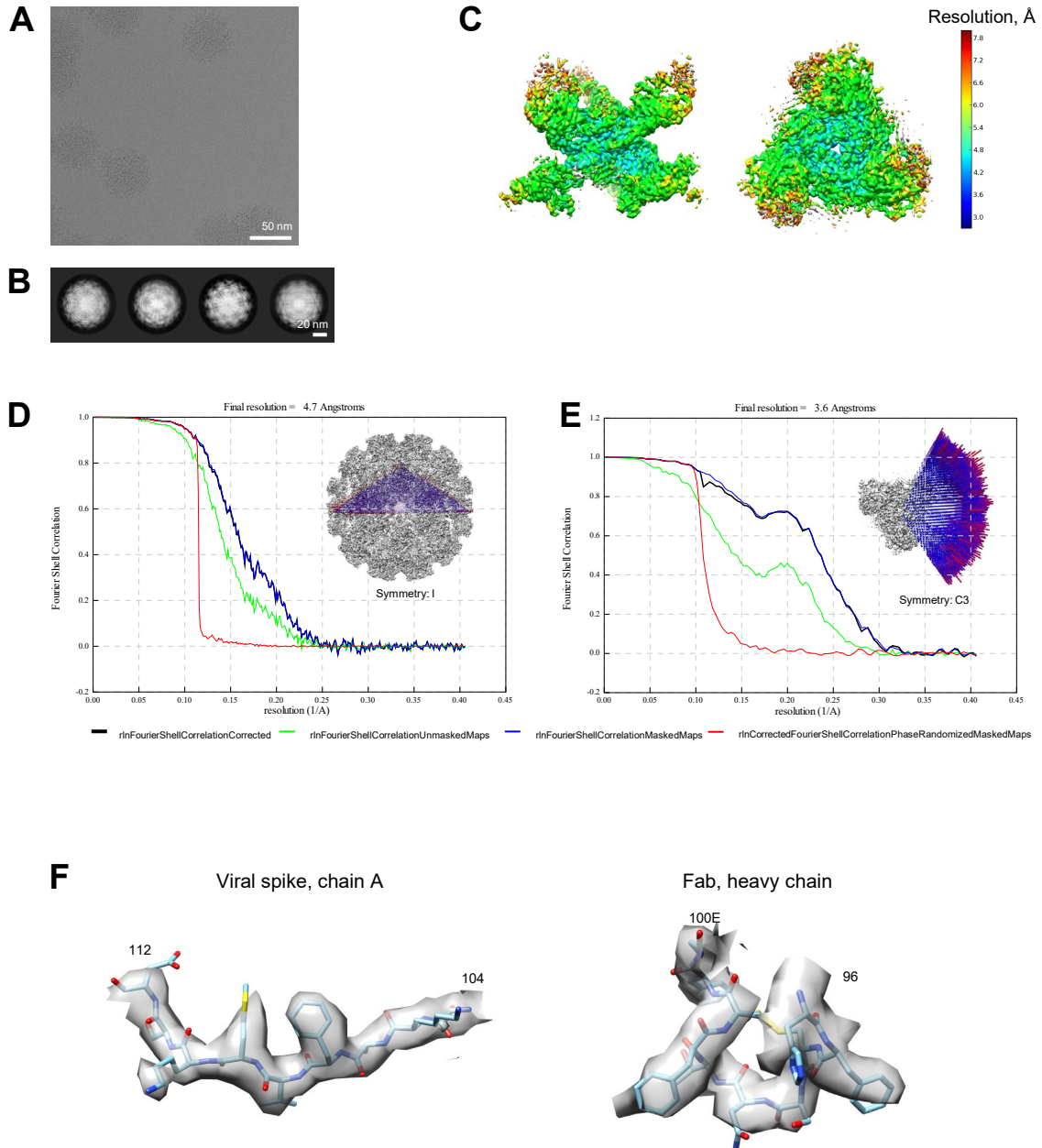
Viral spike, chain A

112

104

Fab, light chain

63

55

**Data S1. Cryo-EM validation of SKT05-VEEV VLP, related to Figures 4-6.**
(A) Representative micrograph. (B) Representative 2D class averages. (C) Local resolution map. (D, E) Gold-standard Fourier shell correlation curves for the entire complex (D) and locally refined structure of one viral spike with one bound Fab (E) as generated by RELION. Insets show the corresponding angular distributions of 2D views. (F) Cryo-EM density for selected representative regions of the locally refined structure.

**A**

**B** 20 nm

**C** Resolution, Å

**D** Final resolution = 4.7 Angstroms

Symmetry: I

**E** Final resolution = 3.6 Angstroms

Symmetry: C3

— rlnFourierShellCorrelationCorrected    — rlnFourierShellCorrelationUnmaskedMaps    — rlnFourierShellCorrelationMaskedMaps    — rlnCorrectedFourierShellCorrelationPhaseRandomizedMaskedMaps

**F**

Viral spike, chain A

Fab, heavy chain

**Data S1. Cryo-EM validation of SKT20-VEEV VLP, related to Figures 4-6.**
(A) Representative micrograph. (B) Representative 2D class averages. (C) Local resolution map. (D, E) Gold-standard Fourier shell correlation curves for the entire complex (D) and locally refined structure of one viral spike with three bound Fabs (E) as generated by RELION. Insets show the corresponding angular distributions of 2D views. (F) Cryo-EM density for selected representative regions of the locally refined structure.